

Research Article

Xiaodong Yang*, Hai Li, Qunfeng Dong, and Shenhe Ren

Research on attenuation motion test at oblique incidence based on double-N six-light-screen system

<https://doi.org/10.1515/phys-2022-0222>

received August 26, 2022; accepted December 15, 2022

Abstract: To improve the photoelectric test accuracy of moving objects, in this study, the speed attenuation caused by air resistance was introduced into the double-N six-light-screen test system, and the test system was theoretically analyzed through oblique incidence with field experiment for verification. It was found in the study that the optimal test values for yaw angle, pitch angle, axial speed, and distance could be obtained by selecting the pulse time origin at the center of two light screen groups. In addition, mud pellets were used for field experiments to effectively verify the simulation results. In a new model, the test accuracy of yaw angle and pitch angle was greatly improved when compared with traditional processing methods, but the laws of error distribution remained almost unchanged. The error of axial speed showed monotonicity as affected by the pitch angle. At the same time, the error of test distance remained symmetric with the improved accuracy, thereby meeting the statistical test requirements for small-volume moving objects.

Keywords: speed attenuation, oblique incidence, pulse time axis, photoelectric test system, Yaw angle, pitch angle

1 Introduction

Air resistance is an important factor affecting the motion speed attenuation of objects [1,2], and the attenuation coefficient directly reflects the degree of speed attenuation. Therefore, the laws of speed change in moving objects can be analyzed by the real-time changes in attenuation coefficient. An in-depth analysis of the laws of speed attenuation can help improve the theoretical accuracy of the photoelectric test system.

The double-N six-light-screen system [3,4] is a typical passive photoelectric test device for accuracy testing on motion speed and motion trajectory of objects with natural background light as a light source. When an object passes through the system's light screens, a time pulse signal will be generated as the flux of light into the diaphragm is changed to calibrate the passing time. Plane parametric equations were used to find out the trajectory and speed of the object's motion, while the yaw angle and pitch angle reflected the object's spatial angles of motion. Traditional processing methods of the test system do not take into account the speed attenuation caused by air resistance and approximate the motion to be uniform rectilinear, in order to establish photoelectric test models for different screen structures [5–11]. In recent years, light-screen test systems have slowly developed and few of them have been improved and optimized through theoretical errors of the test. The speed attenuation of moving objects is one of the important factors that cause theoretical errors, so it is necessary to conduct an in-depth analysis on this subject.

Using oblique incidence as an example, in this study, the attenuation coefficient was introduced into the double-N six-light-screen system. It was found from the test results that the differences in the origin selection for the coordinate axis of pulse time would directly affect the test accuracy of the system. Mass data were organized and sorted to find the optimal position of origin selection for the coordinate axis, which was verified by theoretical simulations and field experiments. This study is of great

* **Corresponding author: Xiaodong Yang**, College of Physics and Electronic Engineering, Xianyang Normal University, Wenlin Road, Weicheng District, Xianyang City, Shaanxi Province, 712000, China, e-mail: kevin09409@sina.com

Hai Li: School of Optoelectronics and Engineering, Xi'an Technological University, University Middle Road No. 2, Weiyang District, Xi'an, Shaanxi Province, 710021, China

Qunfeng Dong, Shenhe Ren: College of Physics and Electronic Engineering, Xianyang Normal University, Wenlin Road, Weicheng District, Xianyang City, Shaanxi Province, 712000, China

practical significance for the optimization of photoelectric test systems for moving objects.

2 Methodology

The double-N six-light-screen system is composed of two three-light-screen groups. For the convenience of calculation, the two light-screen groups [12] are usually adjusted at the same height, as shown in Figure 1. When a moving object passed through this test system, six pulse signals were generated through each light screen to calibrate the passing time of the corresponding screen. Plane parametric equations were built to find this out by testing several physical quantities such as angle of motion, speed, and distance.

When testing the system, it is generally considered that the vertical displacement deviation caused by gravity can be neglected in a limited test interval, while the trajectory of motion is regarded as rectilinear. In traditional methods, speed attenuation caused by air resistance is neglected, and the objects are regarded to be moving uniformly. With respect to objects moving at a high speed, especially those with a large windward area, it is considered

that they have uniform speed, and will therefore result in significant theoretical errors. When an object with m as the mass and S as the windward area moves in the air, air resistance will cause the moving object to accelerate in an opposite direction, and the accelerated speed will be affected by the resistance coefficient C [13].

$$a = C \frac{\rho S v^2}{2m}, \tag{1}$$

where ρ refers to the air density and v refers to the instantaneous speed of the moving object, while $B = \frac{C\rho S}{2m}$ is the speed attenuation coefficient. It was found in this study that when the initial speed of object motion v_0 was less than the speed of sound, the resistance coefficient was almost unchanged and could be regarded as a constant under normal conditions. The time integral was calculated by both sides of the above equation as follows:

$$v = \frac{1}{\frac{C\rho S t}{2m} + \frac{1}{v_0}}. \tag{2}$$

If the test distance is S_0 , the attenuation coefficient can be expressed as follows:

$$B = \frac{1}{S_0} \times \ln\left(\frac{v_0}{v'}\right), \tag{3}$$

where v' refers to the end speed. The attenuation coefficient directly reflects the initial conditions of the flying test on objects and is critical for determining the real-time speed and time of the target fall.

In the traditional processing of the double-N six-light-screen system, the origin is generally selected on the first screen, and the pulse time axis perpendicular to the first screen is used to indicate the pulse time of passage through each light screen. In order to fit the measurement position of the initial velocity v_0 , sometimes the coordinate origin is set in the determined position in front of the first scene, with the common distance of 2 and 4 m. Then, through the calculation of the plan

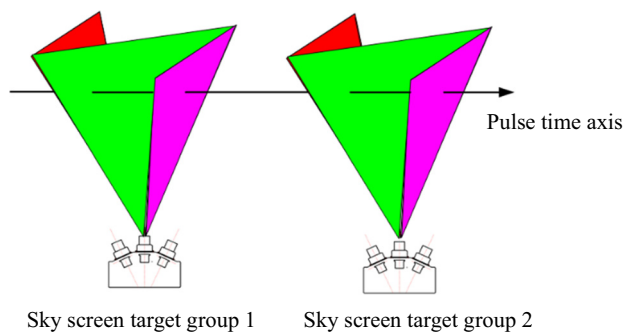


Figure 1: Screen side view of double-N six-light-screen.

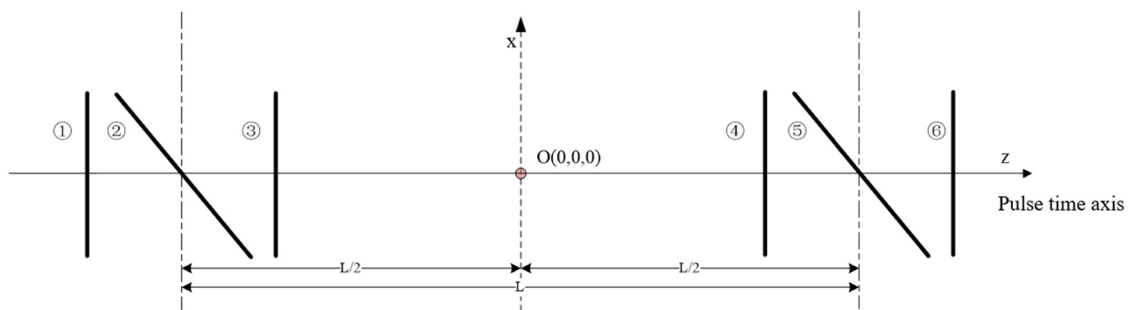


Figure 2: Schematic diagram of azimuth selection for the pulse time origin of double-N six-light-screen system.

parametric equations, the parameters of moving objects to be tested are finally obtained. When the speed attenuation was taken into account and, referring to numerous theoretical studies and data tests, the time origin was selected at the distance center of two light screen groups and the azimuth of the pulse time axis remained unchanged, the analysis results would be more accurate, as shown in Figure 2.

In the new model with the origin at the distance center of two light-screen groups, when an object is obliquely incident on the first screen at $\pm 5^\circ$ in both yaw direction and pitch direction, the test error in axial speed of the moving object with the changes in the distance between the two light-screen groups is shown in Figure 3.

It was seen that when it was closer to the origin of the pulse axis, the test error of axial speed was smaller, and the minimum error was at the origin. In contrast, the changes in distance between the light-screen groups had almost no effect on the axial speed. When the distance between the light-screen groups was set to 4 m, a commonly set distance in field experiments, the influences of yaw angle and pitch angle on the test error in axial speed of the moving object are shown in Figures 4 and 5.

The simulation results show that the yaw angle and pitch angle of a moving object had almost no influence on the axial speed in the smaller angle range, and the minimum error was still at the origin of the pulse axis. The establishment of the pulse axis and the selection of the origin would cause differences in the plane parametric equations corresponding to the system and lead to different test results eventually obtained. In the new model, the error distribution of axial speed showed good regularity, so multiple sets of data could be obtained by

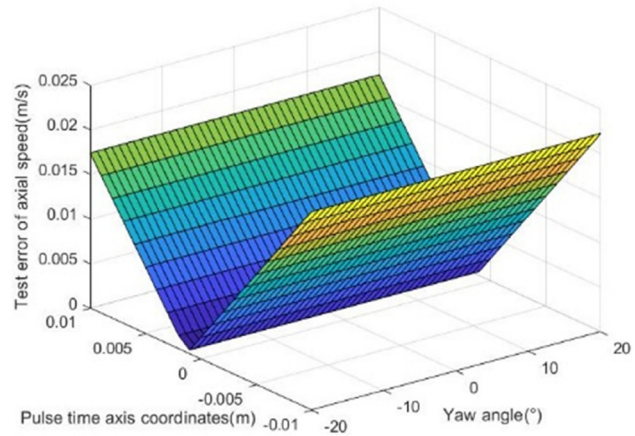


Figure 4: Influence of yaw angle on the test error of axial speed.

adjusting the axial distance of light-screen groups in the process of field building for the system in order to conduct a comprehensive analysis. Moreover, due to the multiple instabilities of the emitter, inevitably, there will be some random angle errors in the yaw direction and pitch direction. An in-depth study of test parameter errors is conducive to the comprehensive performance analysis of the system.

3 Experimental procedures

To facilitate the observation of the laws of error distribution, the initial condition was set as $B = 0.002 \text{ m}^{-1}$, and the initial speed was set as $v_0 = 100 \text{ m s}^{-1}$, while the distance between the two light-screen groups was set as 4 m. When the adjustment range of the pitch angle was

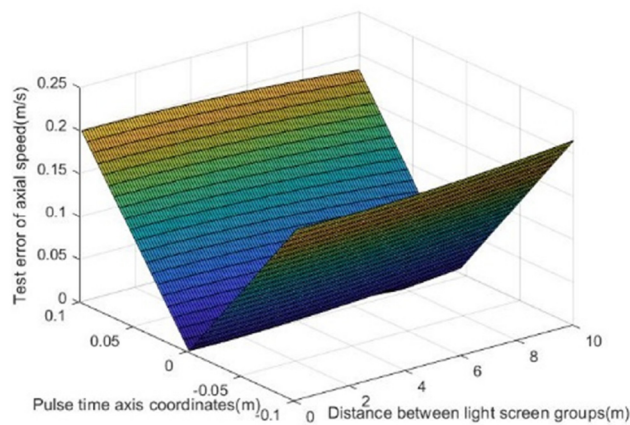


Figure 3: Influence of pulse time axis coordinates and distance between light-screen groups on the test error of axial speed.

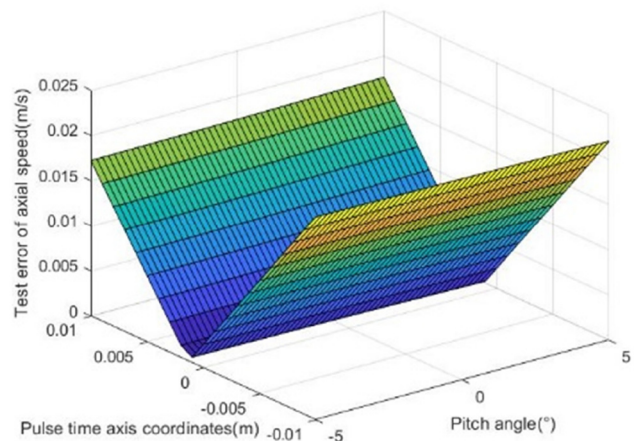


Figure 5: Influence of pitch angle on the test error of axial speed.

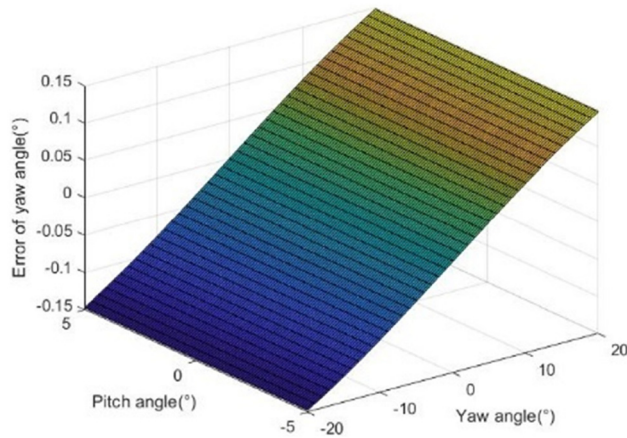


Figure 6: Error of yaw angle in a traditional model.

$\pm 5^\circ$ and that of the yaw angle was $\pm 20^\circ$, the errors of traditional processing methods in the test angle are shown in Figures 6 and 7.

The error of yaw angle was almost unaffected by the pitch angle and increased with an increasing yaw angle. The error of pitch angle was very weakly affected by the yaw angle. The error of pitch angle within the range of yaw angle $\pm 20^\circ$ and pitch angle $\pm 5^\circ$ only showed a weakening fluctuation of 0.01° , which was not symmetrical in the pitch direction. In the process of oblique incidence at a small angle during the field experiment, the error of pitch angle caused by the yaw angle was generally ignored to simplify the processing. As the pitch angle increases, the error of pitch angle increases. Furthermore, the laws of angle error distribution were nearly the same as in the event of normal incidence of an object. The distributions of test angle errors when a new model was adopted and the initial conditions remained unchanged are shown in Figures 8 and 9.

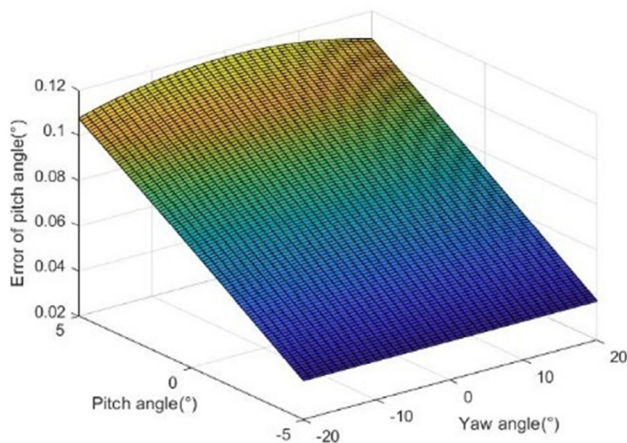


Figure 7: Error of pitch angle in a traditional model.

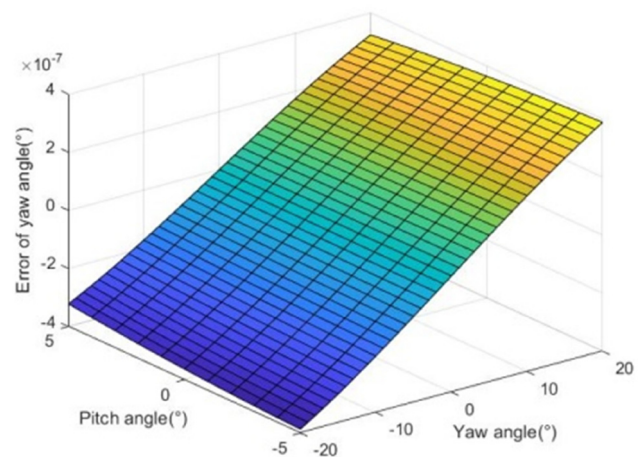


Figure 8: Error of yaw angle in a new model.

The curved surface distribution patterns of these two processing methods with respect to angle fluctuations were extremely similar. Although the angular errors in these two directions in a new model showed no obvious statistical rules, the errors could be controlled at the degree of 10^{-7} within the same range of incidence angle, and the test accuracy was significantly improved.

While an object was approximated to be moving uniformly in a straight line in the screen test range, which meant that the speed attenuation caused by air resistance was neglected, the error of axial speed at oblique incidence with traditional processing methods reached the magnitude of 10^{-2} m s^{-1} , and the error of test distance reached the magnitude of a few tenths of a meter. When the initial conditions remained the same as above, traditional methods of processing were still adopted after the introduction of the attenuation coefficient. In addition,

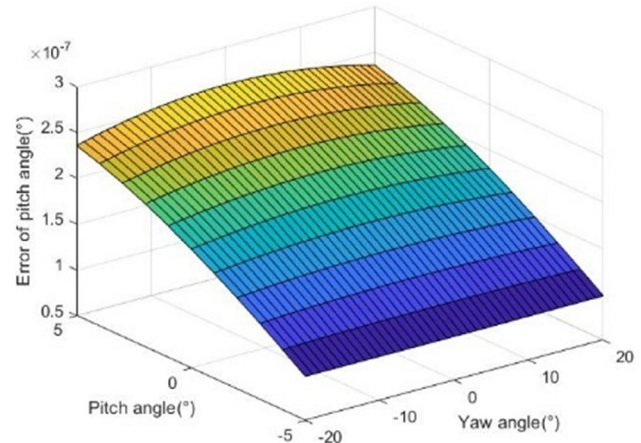


Figure 9: Error of pitch angle in a new model.

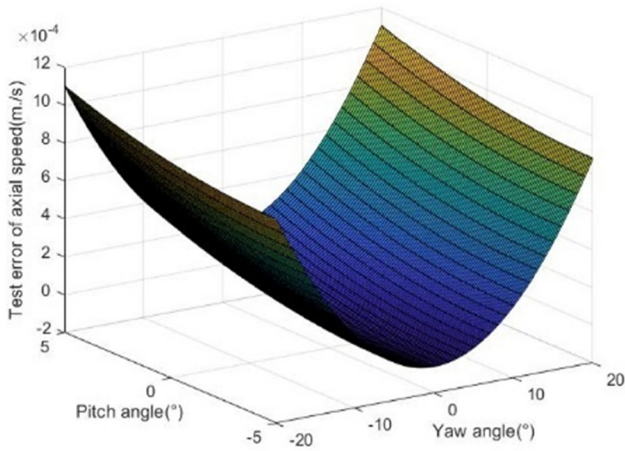


Figure 10: Error of axial speed in a traditional model.

the errors of speed and distance were observed, as shown in Figures 10 and 11.

It could be seen from the figures above that the errors of axial speed and distance could be improved by 1–2 orders of magnitude within the set angle range, and the influence of pitch angle on these two types of errors was relatively weak. At a yaw angle of 0°, the minimum values of errors in axial speed and distance could be obtained, and the two types of errors gradually increased with the increase in the yaw angle. With a test distance of 8 m, the relative error of axial speed was not higher than 0.01, while that of test distance was not higher than 0.008. When the range selection for the angle of incidence and the initial conditions remained unchanged, the new model was adopted for processing, and the errors of axial speed and distance are shown in Figures 12 and 13.

In the new model, the error of axial speed was mainly affected by the pitch angle and showed monotonicity,

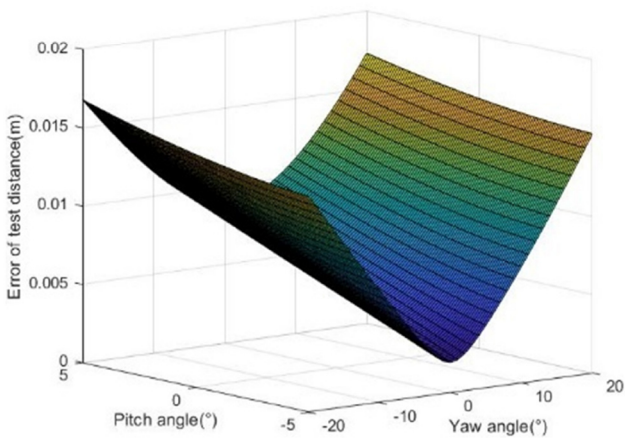


Figure 11: Error of test distance in a traditional model.

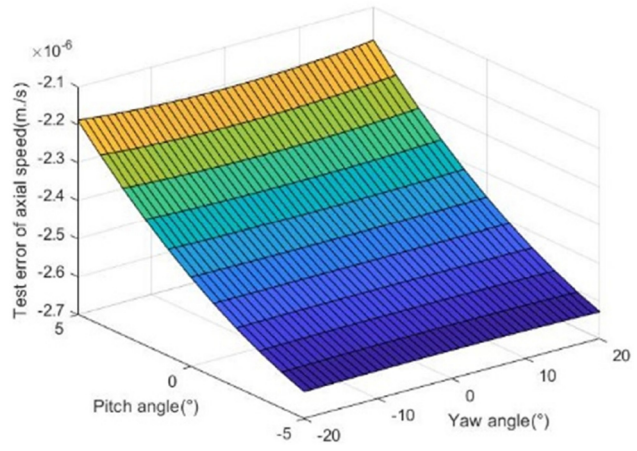


Figure 12: Error of axial speed in a new model.

while the yaw angle had almost no effect on the error of axial speed. Within the angle range, the error of axial speed was three orders of magnitude higher than that in traditional processing methods, and the error of distance was about six orders of magnitude higher than that in traditional processing methods with extremely similar laws of error distribution to those in traditional methods. The minimum error was still at a yaw angle of 0°. Taking the test distance of 8 m as an example, the relative error of the test distance was not higher than 0.2×10^{-7} , which could ensure the test accuracy of small-volume moving objects.

To effectively verify the simulation results, many field experiments were carried out on sunny and windless days. Spherical mud pellets were selected as the test objects for such experiments, and the mass and windward area were changed to analyze the errors of screen coordinates and speed, intuitively reflecting the advantages of the new

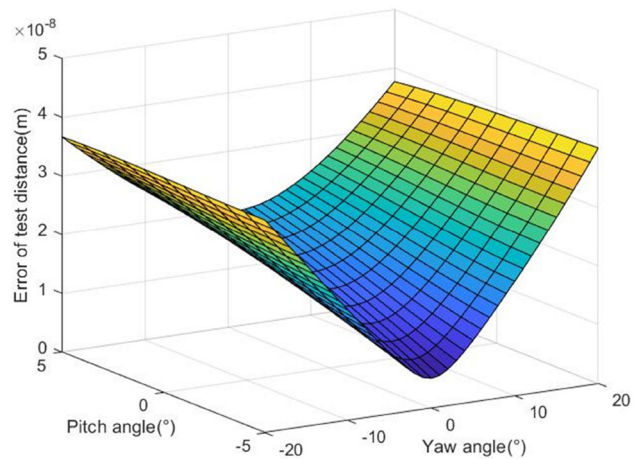


Figure 13: Error of test distance in a new model.

Table 1: Average values of pulse time calibration and B in a traditional model

S No	t_1 (s)	t_2 (s)	t_3 (s)	t_4 (s)	t_5 (s)	t_6 (s)	B (m^{-1})
1	0	1.659	3.102	33.441	37.105	39.593	0.011
2	0	2.871	5.978	37.182	42.118	45.866	0.009
3	0	2.656	4.543	33.674	38.826	41.574	0.010
4	0	3.022	5.525	32.974	35.974	38.221	0.009
5	0	2.996	4.916	34.182	39.014	43.003	0.009
6	0	2.737	5.881	35.733	39.855	32.957	0.010
7	0	2.953	5.638	32.359	36.638	39.843	0.011
8	0	3.468	5.912	35.988	39.736	42.088	0.012

model compared with traditional processing methods. In the event that the selected distance between light-screen groups remained unchanged, the initial conditions were used to find the real-time attenuation coefficient based on Formula (3). With 3,966 mm as the distance between light-screen groups, 78.5 mm² as the windward area of mud pellets, and 5° as both the incident yaw angle and pitch angle, the average values of the pulse time calibration and B obtained through traditional processing methods for six screens are shown in Table 1. The test coordinates were compared with the reference standard values obtained through vertical plane coordinates to find out the horizontal

and vertical positional deviations. Meanwhile, the test speed of the mud pellets was compared to the reference standard value of speed obtained by theoretical derivation to find the relative speed deviation, as shown in Table 2.

In Table 2, δx and δy refer to the horizontal positional deviation and vertical positional deviation, respectively, obtained by subtracting the statistical average from the difference between the test value and the reference standard value. Δv refers to the difference between the test speed and the reference standard speed. Under the same setting conditions, the new model was adopted for recalibration of the pulse time, and the average value of B was calculated, as shown in Table 3. The test coordinates and speed were compared with the corresponding standard values to find the relative deviations, as shown in Table 4.

From experimental data, it was clear that the test results obtained by the new model were more accurate than those obtained by the traditional method. As the field experiments were affected by more complicated external factors, it was inevitable that there would be some deviations between the data obtained and the theoretical values, but the new model could still show significant advantages. The horizontal and vertical average positional deviations in the traditional model were 6.51 and 4.96 mm, and the difference between the test speed

Table 2: Statistics of test data corresponding to Table 1

S No	x_m (mm)	y_m (mm)	x_0 (mm)	y_0 (mm)	δx (mm)	δy (mm)	v_m ($m s^{-1}$)	v_0 ($m s^{-1}$)	δv ($m s^{-1}$)
1	-110.0	-170.8	-297.5	-318.5	-7.30	2.90	99.91	99.90	-0.01
2	172.3	-298.7	-25.0	-437.0	2.50	-6.50	135.95	135.97	0.02
3	348.2	-144.0	143.0	-294.0	10.40	5.20	125.61	125.62	0.01
4	373.3	-56.2	171.5	-203.5	7.00	2.50	130.07	130.11	0.04
5	-71.7	119.3	-273.5	-33.0	7.00	7.50	132.85	132.88	0.03
6	237.8	128.4	39.0	-26.0	4.00	9.60	124.94	124.92	-0.02
7	-204.9	18.9	-394.0	-132.0	-5.70	6.10	123.84	123.81	-0.03
8	206.7	-118.5	15.0	-264.0	-3.10	0.70	125.18	125.19	0.01

Table 3: Values of pulse time calibration and B in the new model

S No	t'_1 (s)	t'_2 (s)	(s)	t_c (s)	t'_4 (s)	t'_5 (s)	(s)	B (m^{-1})
1	-21.325	-19.012	-16.929	0	15.371	18.123	20.602	0.010
2	-24.063	-19.345	-17.583	0	15.988	18.662	21.113	0.011
3	-24.445	-21.037	-18.681	0	17.723	20.506	23.486	0.013
4	-25.817	-22.164	-17.334	0	15.962	19.054	21.502	0.010
5	-26.008	-22.869	-19.812	0	18.775	20.979	23.476	0.009
6	-27.986	-24.641	-20.044	0	18.847	21.351	23.817	0.009
7	-30.162	-27.513	-23.979	0	22.152	25.657	28.003	0.009
8	-24.579	-21.991	-18.653	0	16.867	19.206	21.819	0.011

Table 4: Statistics of test data corresponding to Table 3

S No	(mm)	y'_m (mm)	x'_0 (mm)	y'_0 (mm)	$\delta x'$ (mm)	$\delta y'$ (mm)	v'_m (m s ⁻¹)	v'_0 (m s ⁻¹)	$\delta v'$ (m s ⁻¹)
1	-106.361	-209.468	-297.5	-318.5	-1.76	5.73	99.911	99.912	0.001
2	166.623	-334.385	-25.0	-437.0	-1.28	-0.68	135.965	135.965	0
3	334.081	-186.931	143.0	-294.0	-1.82	3.77	125.617	125.616	-0.001
4	362.271	-105.136	171.5	-203.5	-2.13	-4.94	130.076	130.077	0.001
5	-71.384	71.681	-273.5	-33.0	9.22	1.38	132.846	132.846	0
6	228.523	73.652	39.0	-26.0	-3.38	-3.65	124.932	124.932	0
7	-195.774	-27.941	-394.0	-132.0	5.33	0.76	123.837	123.839	0.002
8	204.341	-161.065	15.0	-264.0	-3.56	-0.37	125.184	125.183	-0.001

and the reference standard speed was 0.00625 on average, while the horizontal and vertical average positional deviations in the new model were 4.63 and 3.53 mm, effectively improving the error of the test distance, and the difference between the test speed and the reference standard speed was 0.00025 on average, one order of magnitude higher than the traditional method. To conveniently, quickly, and intuitively verify the test accuracy of yaw angle and pitch angle, the photovoltaic conversion data acquisition and analysis system could be used to visualize the test results, and the system test interface is shown in Figure 14.

In Figure 14, t_0-t_6 correspond to seven pulse times, respectively; B is the attenuation coefficient; L is the distance between two light-screen groups; S is the distance from the receiving light screen to the second screen; h is the height difference between two light-screen groups; x and y are the abscissa and ordinate of the receiving light screen, respectively; v is the velocity of the object.

To sum up, the experimental data remained highly consistent with the theoretical simulation results, which could verify the advantages of the new model when processing test data. To ensure method optimization, in addition to the calibration of the pulse time origin in the traditional and new models, positions were selected randomly on the pulse axis, and the obtained test results could not meet the requirements of the new model, with a large difference in accuracy.

4 Conclusion

With the oblique incidence of the double-N six-light-screen test system taking into account the speed attenuation, there will be relatively significant differences between the parameters to be tested with the differences in position selection for the pulse time origin. It was eventually found that the minimum error for test parameters can be obtained through the new processing method with the pulse time origin at the center of two light screens. Through theoretical simulation and comparison, it is concluded in this study that the errors of yaw angle and pitch angle obtained by the new model were 7–8 orders of magnitude higher than those obtained by the traditional method, but the laws of error fluctuation remain unchanged in general. Furthermore, the error of axial speed was improved by 2–3 orders of magnitude, showing monotonicity with the changes in pitch angle. The error of distance was increased by 5–6 orders of magnitude, showing apparent symmetry centered on zero value of yaw angle. To verify the theoretical values, mud pellets of different masses and windward areas were used for field experiments at an oblique incidence of 5° in yaw and pitch directions, and the obtained laws were consistent with the theoretical analysis. It can be seen that the establishment and solution of plane parametric equations for the photoelectric test system of moving objects are highly dependent on the calibration of pulse time.

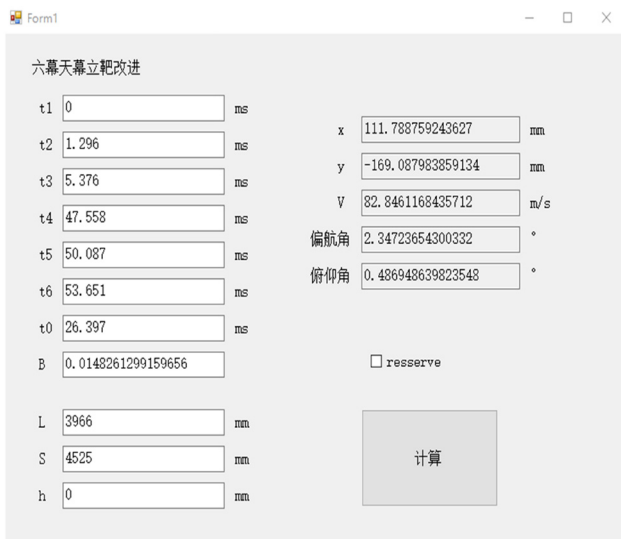


Figure 14: Interface of photovoltaic conversion data acquisition and analysis system.

With the in-depth study on the test of moving objects by light-screen systems, in addition to considering the speed attenuation caused by air resistance, other factors such as object rotation, gas pressure difference, and temperature will be introduced into the analysis of the test system in the future, making the photoelectric test system more accurate.

Funding information: This study was supported by the Key Cultivation Project of Scientific Research Program of Xianyang Normal University (Grant No. XSYK21040).

Author contributions: All authors have accepted responsibility for the entire content of this manuscript and approved its submission.

Conflict of interest: The authors state no conflict of interest.

References

- [1] Huang C, Liu Z, Liu ZX, Hao CL, Li DJ, Luo K. Motion characteristics of high-speed supercavitating projectiles including structural deformation. *Energies*. 2022;15(1):1–7.
- [2] Astakhov SA, Biriukov VI. Problems of ensuring the acceleration dynamics of aircraft during track tests at a speed of 1600 m/s. *Incas Bull*. 2020;12(S):33–42.
- [3] Li H, Ni JP, Yang XD, Dong QF. Test influence of screen thickness on Double-N Six-light-screen sky screen target. *Open Phys*. 2022;19(1):1–8.
- [4] Chen R, Ni JP, Liu JL. Uncertainty analysis of coordinate measurement of Six-light-screen array sky screen vertical target based on engineering model. *Acta Armamentarii*. 2019;40(3):612–20.
- [5] Li H, Zhang X, Zhang X, Lu L. Detection sensitivity correction calculation model and application of photoelectric detection target in Four-screen intersection testing system. *Measurement*. 2021;177(3):109281.
- [6] Liu YW, Jiang M, Zhang ZY, Li Y. Study on aerodynamic characteristics of projectile in plateau based on shooting test. *J Ordnance Equip Eng*. 2019;40(6):1–4.
- [7] Wu Z, Zhang X. On-site calibration method of target distance of the sky screen target velocity measuring system. *Optik*. 2019;178:483–7.
- [8] Dong T, Ni JP. Measurement principle of six-light-screen vertical target based on sky screen. *J Appl Opt*. 2011;32(5):913–6.
- [9] Cheng-Gang LU, Wang YJ, Yao ZJ, Zhang L, Fan B. Attack angle measurement of projectile with multi-linear array photoelectric vertical target. *Transducer Microsyst Technol*. 2016;35(5):32–5.
- [10] Shi L. *Research on the Technology of Integrated Receiving-Transmitting Laser Screens*. Xi'an: Xi'an Technological University; 2010.
- [11] Zhang YW, Zhang S, Zhang MY, Zhang HZ. Intelligent light screen target coordinate measurement system, CN210570247U; 2020.
- [12] Ni JP. *Technol application Meas Light Screen Array*. Beijing: National Defense Industry Press; 2014. p. 176–85.
- [13] Liu PQ. *Aerodynamics*. Beijing, China: Science Press; 2022. p. 35–61.